Dalton Transactions

Accepted Manuscript

ROYAL SOCIETY OF CHEMISTRY

www.rsc.org/dalton

Journal Name

ARTICLE

Substituent effect and wavelength dependence of the photoinduced Ru-O homolysis in the $[Ru(bpy)_2(py\text{-}SO_3)]^+$–type complexes

Received 00th January 20xx,
Accepted 00th January 20xx

DOI: 10.1039/x0xx00000x

www.rsc.org/

*Yue Zheng,[ab] Qian-Xiong Zhou,[*a] Yang-Yang Zhang,[ab] Chao Li,[a] Yuan-Jun Hou[a] and Xue-Song Wang[*a]*

$[Ru(bpy)_2(py\text{-}SO_3)]^+$ (**3,** bpy = 2,2'-bipyridine, py-SO_3 = pyridine-2-sulfonate) was recently found to undergo py-SO_3 ligand dissociation and py-SO_3• radical generation in hypoxic conditions upon irradiation (*Chem. Commun.,* 2015, **51**, 428). To explore the substituent effect on the Ru-O homolysis by which the py-SO_3• radical may be produced, $[Ru(4,4'\text{-}(R)_2\text{-}bpy)(py\text{-}SO_3)]^+$, where R = OCH_3 (**1**), CH_3 (**2**), $COOCH_3$ (**4**), were synthesized and their photochemical properties were investigated. The py-SO_3• radical generation efficiencies followed the order of **4 > 3 > 2 > 1**, and the radical generation efficiencies are wavelength dependent. As a result, **3** and **4** may lead to DNA covalent binding and DNA cleavage upon 355 nm irradiation, but merely DNA covalent binding upon 470 nm irradiation. In contrast, **1** and **2** can serve as DNA photo-binding agents only due to their less efficient Ru-O homolysis. The Ru-O homolysis via the $^3\sigma(Ru\text{-}O)\pi^*(R\text{-}bpy)$ state is proposed to rationalize the substituent effect and the wavelength dependence, which is supported by TD-DFT calculations. This work gave insights into the mechanism of the Ru-O homolysis and provided guidelines for developing new $[Ru(bpy)_2(py\text{-}SO_3)]^+$–type complexes with higher Ru-O homolysis efficiency. Such complexes have dual activities of photoactivated chemotherapy (PACT) and photodynamic therapy (PDT) in hypoxic conditions and are therefore promising as a new class of antitumor drugs.

Introduction

As one of the most famous metallodrugs, cisplatin, *cis*-$Pt(II)(NH_3)_2Cl_2$, has been clinically used for decades for the treatment of many types of cancers. However, its efficacy is limited severely by the notorious side effects, such as neuro-, hepato- and nephrotoxicity, as well as the inherent and acquired drug resistance.[1] To circumvent these problems, many efforts have been devoted to Pt(IV) prodrugs that can release cytotoxic Pt(II) species either triggered by tumor-related factors, such as the reducing intracellular environment,[2] or upon exposure to external stimuli, such as, photoirradiation.[3] By spatial and temporal control of irradiation, the Pt(IV)-based photoactivated chemotherapy (PACT) agents may confine their toxicities within the diseased sites. One prominent example is *trans*, *trans*, *trans*-$[Pt(N_3)_2(OH)_2(NH_3)(py)]$ (py = pyridine), which is stable in the dark and non-toxic, but becomes 80-fold more toxic toward cancer cells than cisplatin after photoinduced ligand substitution and reduction reactions.[3d]

In the development of new anticancer metallodrugs, another big family of complexes, Ru(II) and Ru(III) complexes,[4] are drawing increasing attention by virtue of their favorable ligand exchange kinetics and their ability to mimic iron in binding biomolecules which renders them lower toxicity.[5] Similar to their Pt(IV) counterparts, many Ru(II) complexes with photolabile ligand(s) can bind DNA covalently after photoinduced ligand dissociation and therefore are promising as new types of PACT agents.[6] More intriguingly, for some Ru-based PACT agents, the photolabile ligand itself is the anticancer species, leading to the so called dual-activity PACT agents in which two or even more anticancer active species are released upon irradiation.[7] In recent years, several Ru(II)-based PACT agents with diimine ligand of large π conjugation structure were found to be able to generate singlet oxygen ($^1O_2$) along with ligand photodissociation.[8] $^1O_2$ is a kind of reactive oxygen species (ROS) which accounts for the anticancer activities of many photosensitizers in photodynamic therapy (PDT), another type of photoactivation cancer treatment modality that has got clinical applications.[9] Due to the multiple-targeting character of ROS, the combination of PACT with PDT may improve anticancer activities of the corresponding complexes and restrict drug resistance. Very

[a] *Key Laboratory of Photochemical Conversion and Optoelectronic Materials, Technical Institute of Physics and Chemistry, Chinese Academy of Sciences, Beijing 100190, P. R. China; E-mail: xswang@mail.ipc.ac.cn and zhouqianxiong@mail.ipc.ac.cn*

[b] *Graduate School of Chinese Academy of Sciences, Beijing 100049, P. R. China.*

† Electronic Supplementary Information (ESI) available: Absorption spectra changes of **1-3** in H_2O in the dark or upon irradiation at λ = 470 nm, theoretical calculations and DNA gel electrophoresis in varied conditions, high-resolution ESI MS and ^1H NMR spectra of **1-4**. See DOI: 10.1039/b000000x/

recently, we designed and synthesized a new Ru(II) complex, $[Ru(bpy)_2(py\text{-}SO_3)]^+$ (bpy = 2,2'-bipyridine, py-SO_3 = pyridine-2-sulfonate, complex **3** in Scheme 1).[10] Preliminary study showed that it may at least partly undergo homolysis of Ru-O bond upon irradiation, leading to the dissociation of py-SO_3 from Ru center and meanwhile the generation of py-SO_3· radicals (Scheme 1). The py-SO_3· radicals are so reactive to be capable of producing hydroxyl radical (·OH) by reaction with water, a kind of more potent ROS than $^1O_2$.[10] As a result, $[Ru(bpy)_2(py\text{-}SO_3)]^+$ can photobind and photocleave DNA simultaneously, displaying dual activities of PACT and PDT also.[10] In sharp contrast to $^1O_2$, the generation of py-SO_3· and ·OH by $[Ru(bpy)_2(py\text{-}SO_3)]^+$ is an oxygen independent process, making the dual-activity feature remain even in hypoxic conditions that many types of cancer cells exist in. Additionally, ligand dissociation and $^1O_2$ generation are usually competitive, *i.e.* the enhancement in ligand dissociation often accompanies the decline in $^1O_2$ generation or vice versa.[8] Such a compromise is not present in $[Ru(bpy)_2(py\text{-}SO_3)]^+$, where promotion of Ru-O bond homolysis and ROS generation will also facilitate ligand dissociation.

Considering the attractive potentials of $[Ru(bpy)_2(py\text{-}SO_3)]^+$ in anticancer applications, particularly against hypoxic tumor cells which can be the most resistant to radiotherapy and chemotherapy and susceptible toward metastasis,[11] it is of significance to understand the mechanism of the photoinduced Ru-O bond homolytic splitting and to develop strategies that may enhance the efficiency of Ru-O bond photo-homolysis. In fact, the thermal homolysis of organo-metal bonds has received extensive and intensive studies for better understanding the role of coenzyme B12 and for fruitful applications as catalysts in organic transformations and controlled radical polymerizations.[12] The photo-induced homolytic cleavage of organo-metal bonds was also found in $[Re(R)(CO)_3(\alpha\text{-diimine})]$ and $[Ru(I)(R)(CO)_2(\alpha\text{-diimine})]$ types of complexes, where R = benzyl, 2-propyl, ethyl or methyl and α-diimine = 4,4'-dimethyl-2,2'-bipyridine or *N,N'*-diisopropyl-1,4-diazabutadiene.[13] One common character in these metal carbonyl complexes is that they all contain a high-lying M-R σ bond and an electron-accepting ligand with an unoccupied π* orbital. The M-R photo-homolysis is generally believed to originate from the reactive σ(M-R)π* excited state, *i.e.* electron excitation from the M-R σ bond to the π* orbital of α-diimine, which may be accessed indirectly via ^{1}MLCT excitation.[13] The Ru-O photo-homolysis in $[Ru(bpy)_2(py\text{-}SO_3)]^+$ might follow the same mechanism and thus any perturbation on either Ru-O σ bond or bpy-based π* orbital may impact Ru-O photo-homolysis. Taking this in mind, we herein explore the substituent effect of the bpy ligand on the Ru-O photo-homolysis of $[Ru(bpy)_2(py\text{-}SO_3)]^+$. Three new Ru(II) complexes, $[Ru(4,4'\text{-}(R)_2\text{-}2,2'\text{-bipyridine})_2(py\text{-}SO_3)]^+$ (R = OCH_3 (**1**), CH_3 (**2**) or $COOCH_3$ (**4**), as shown in Scheme 1) were synthesized and their photophysical, photochemical and photobiological properties were compared in detail with $[Ru(bpy)_2(py\text{-}SO_3)]^+$ (**3**). It was found that the $COOCH_3$ groups can improve Ru-O photo-homolysis effectively, and the underlying mechanism may provide guidelines for developing more potent anticancer agents with dual activities of PACT and PDT.

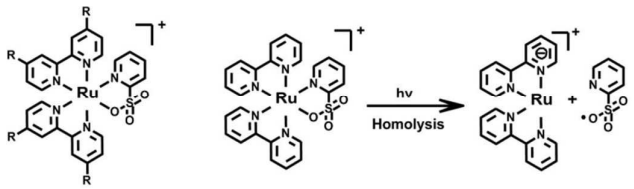

R = OCH_3(**1**), CH_3 (**2**), H(**3**) or $COOCH_3$ (**4**)

Scheme 1. Molecular structures of the examined complexes and the Ru-O homolysis of **3** upon irradiation.

Results and discussion

Absorption, emission and electrochemistry properties

The complexes **1-4** show characteristic R-bpy-based ππ* transitions with maxima at 282, 286, 287, and 311 nm, respectively (Figure 1 and Table 1). The absorption bands at lower energies, *i.e.* longer than 350 nm, may be assigned to $Ru(t_{2g})\rightarrow$R-bpy(π*) ^{1}MLCT with maxima at 467 nm for **1**, 458 nm for **2**, 452 nm for **3**, and 488 nm for **4**. While the electron-donating R groups (OCH_3(**1**) or CH_3(**2**)) lead to a slight bathochromic shift in MLCT absorption onset with respect to **3**, the MLCT red shift is significant in the case of electron-withdrawing R groups ($COOCH_3$(**4**)). Similar behaviors were also found in other Ru complexes while the electron withdrawing groups may red shift ^{1}MLCT more remarkably.[14] Such a red shift is generally attributed to more effective stabilization on R-bpy(π*) than on $Ru(t_{2g})$ by electron-withdrawing groups and more marked destabilization on $Ru(t_{2g})$ than on R-bpy(π*) by electron-donating groups. Besides the lowest-lying ^{1}MLCT, the ^{1}MLCT at higher energies is also observed at 374 nm for **1**, 370 nm for **2**, 362 nm for **3**, and 364 nm for **4,** respectively.

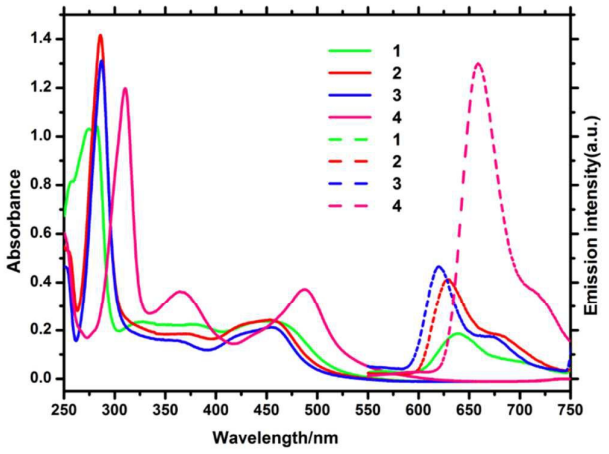

Figure 1. Absorption spectra of **1-4** (25 μM) at 298 K in H_2O (solid line) and their emission spectra (dash line) at 77 K in ethanol/methanol glass (4:1 in volume ratio).

Table 1. Absorption Maxima, Molar Extinction Coefficients, Yields for Product Formation relative to **3**, Oil/Water Partition Coefficients, and Redox Potentials of **1-4**.

complex	λ_{abs}/nm (ε/×10^{3}M^{-1}cm^{-1})[a]	λ_{em}/nm[b]	Φ[c]	log $P_{O/W}$	$E_{1/2}$/V[d]
1	282(41.8) 374(9.0) 467(9.1)	640	0.57	-1.29	+0.84, -1.54, -1.74
2	286(56.7) 370 (7.4) 458(9.6)	630	0.72	-1.01	+0.98, -1.53, -1.75
3	287(52.4) 362 (6.4) 452(8.5)	620	1.00	-2.06	+1.09, -1.42, -1.67
4	311(47.9) 364(14.5) 488(15)	660	0.81	-2.01	+1.31, -0.98, -1.20

[a] in H_2O at 298 K. [b] in ethanol/methanol (4:1) at 77 K. [c] Relative quantum yields *vs.* **3** of the ligand photodissociation, measured in H_2O after 2 min of irradiation at 470 nm. [d] *vs.* SCE and measured in CH_3CN.

Although they are not emissive in H_2O or CH_3CN at 298 K, **1-4** exhibit luminescence at 77 K in ethanol/methanol (4:1, v:v) glasses, as shown in Figure 1. Similar to their absorption spectra, both electron-donating and electron-withdrawing groups make the emission peaks red-shifted than **3** (620 nm), with emission maximum at 640 nm for **1**, 630 nm for **2**, and 660 nm for **4**, respectively.

The complexes **1-4** showed quasi-reversible metal-centered oxidation events, $E_{1/2}(Ru^{3+/2+})$, in the range of +0.84 to +1.31 V *vs* SCE in CH_3CN (Table 1), which are much lower than typical Ru(II) polypyridyl complexes.[15] The less positive oxidation potentials of **1-4** result from the enhanced electron density on Ru provided by the anionic py-SO_3 ligand. The oxidation potentials follow the trend of **1** (+0.84 V) < **2** (+0.98 V) < **3** (+1.09 V) < **4** (+1.31 V), suggesting that the Ru(t_{2g}) orbital is stabilized by the electron-withdrawing groups but destabilized by the electron-donating groups.[14] Upon cathodic scan, **1-4** diplayed reversible R-bpy centered reduction events at -1.54 V for **1,** -1.53 V for **2,** -1.42 V for **3**, and -0.98 V for **4**. Though the substituent effects on R-bpy(π^*) are very similar to that on Ru(t_{2g}), the influence extents are different, making the electrochemical energy gap follow the order of **3** (2.51 eV), **2** (2.51 eV) > **1** (2.38 eV) > **4** (2.29 eV), which is in good agreement with their ^{1}MLCT transition energies.

Photolysis

The photolysis reactions of **1-4** in H_2O were monitored by their absorption spectra changes as a function of irradiation time. Similar to **3** in our previous report,[10] the absorption spectra of **1**, **2** and **4** underwent remarkable changes (Figure 2 and Figure S1-S3) when exposed to visible light irradiation at 470 nm. In all cases, a set of isosbestic points were observed, indicating that one new species formed. This new species has been

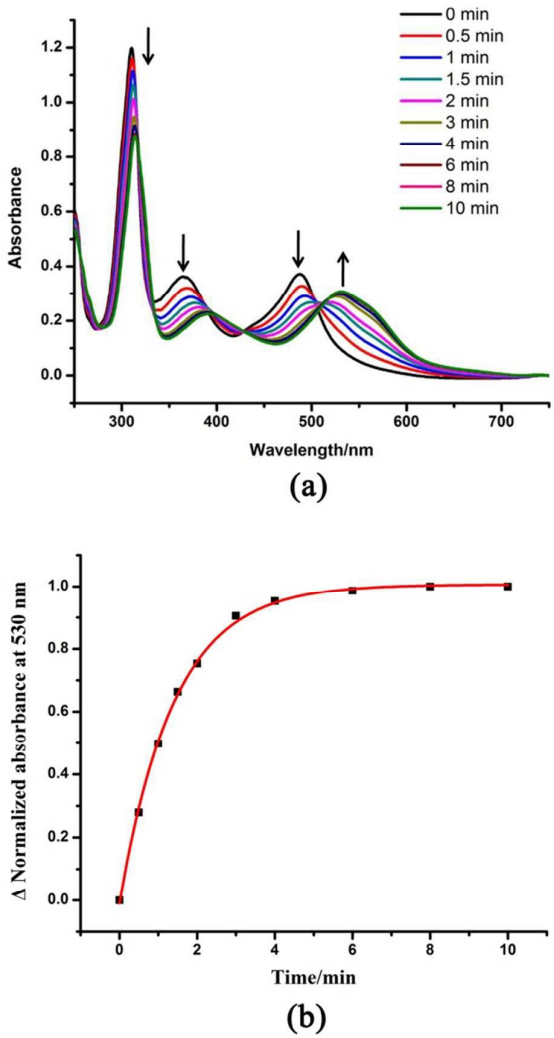

Figure 2. (a) Absorption spectra changes of **4** (25 μM) in Ar-saturated H_2O upon irradiation (470 nm), (b) absorbance changes at 530 nm as a function of irradiation time.

ascribed to $[Ru(bpy)_2(H_2O)_2]^{2+}$ in the case of **3**,[16] which is further confirmed by ^{1}H NMR and high-resolution ESI-MS data.[10] Obviously, all **1-4** can undergo photo-dissociation of py-SO_3 ligand to generate the corresponding $[Ru(R\text{-}bpy)_2(H_2O)_2]^{2+}$ complex with ^{1}MLCT maximum at 502 nm for **1**, 491 nm for **2** and **3** and 530 nm for **4**, respectively. The py-SO_3 ligand dissociation was also found in photolysis of **1-4** in CD_3CN, as shown in their ^{1}H NMR spectra before and after irradiation at 470 nm (Figure S4). When kept in the dark at room temperature, negligible spectra changes were observed over 24 h (Figure S5), demonstrating the favorable stability of **1-4** in the absence of irradiation. By comparing the conversion efficiencies of each complex after 2 min of irradiation (e.g. Figure 2b) and the initial OD values of the irradiated solution at 470 nm, the relative photo-induced ligand dissociation quantum yields are estimated to be 0.57 for **1**，0.72 for **2**, 1.00 for **3** and 0.81 for **4**, respectively. Though the ligand

photodissociation rates are very fast and can finish within 8 min for **1-4**, the substituent effect is still discernible. It is expected that the ligand photodissociation is dependent on how well the two initial fragments diffuse outside of the solvent cage. Therefore, the water solubility of the fragments may play a role in the observed overall yields. We measured oil/water partition coefficients of **1-4** and found they followed the order of **2** > **1** > **4** ≈ **3** (Table 1), not in line with the order of ligand photodissociation efficiencies. This result suggests that water solubility alone cannot explain the substituent effect, which may be the results of many factors, including the population possibility of the ^{3}LF state. The underlying mechanism will be discussed below.

EPR experiments

Different from the typical Ru complexes bearing photolabile ligand,[6-9] **3** may undergoes Ru-O homolysis upon irradiation to generate py-SO_3· radicals, which can be trapped by DMPO, a common spin trapping agent, to show a seven-line EPR signal with an intensity ratio of 1 : 2 : 2 : 2 : 2 : 2 : 1 in CH_3CN, as shown in our previous work.[10] This unique EPR signal is attributable to DMPOX (5,5-dimethyl-2-pyrrolidone-1-oxyl), which is formed by spin trapping of the py-SO_3· radical by DMPO followed by a series of rearrangements.[10,17]

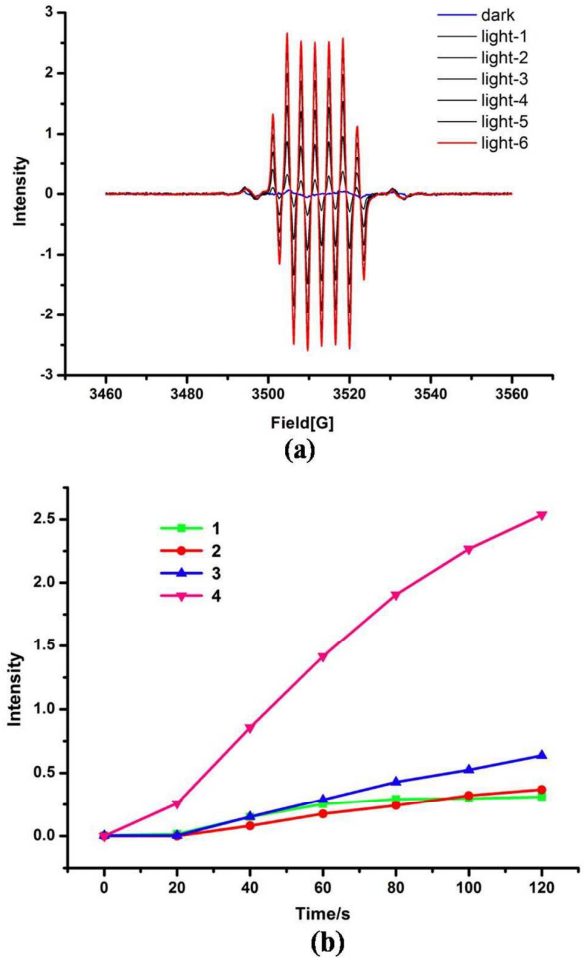

Figure 3. (a) EPR signals obtained upon laser irradiation (355 nm) of an Ar-saturated CH_3CN solution of **4** and DMPO (50 mM). (b) EPR signal intensity changes of **1-4** as a function of irradiation time.

In order to evaluate the contribution of the Ru-O homolysis in the photodissociation of py-SO_3, EPR experiments were carried out in a more quantitative way. The absorbance at 355 nm of all irradiated samples was adjusted to the same and the EPR signal intensities obtained at the same irradiation time were compared. As shown in Figure 3 and Figure S6-S8, a seven-line EPR signal with an intensity ratio of 1 : 2 : 2 : 2 : 2 : 2 : 1 and hyperfine coupling constants of a^N= 7.0 G, $a\gamma^{H1}$ = $a\gamma^{H2}$ = 3.5 G was detected upon irradiation of **1-4** in Ar-saturated CH_3CN, in line with our previous results.[10] The signal intensity follows the trend of **4** > **3** > **2** > 1. If solvent-cage effect play a major role, **1** and **2** should be more efficient than **3** in radical generation, because both of them are more lipophilic than **3** (Table 1) and the EPR experiments were carried out in CH_3CN. Additionally, the similar water/oil partition coefficients of **3** and **4** cannot account for their large disparity in radical generation. Thus, the observed radical generation efficiencies may be mainly the result of electronic effect, *i.e.* the electron-withdrawing substituent ($COOCH_3$) may facilitate the homolysis of Ru-O bond and the electron-donating substituent (OCH_3 or CH_3) suppress this process. This is in good agreement with the assumption that the Ru-O homolysis in **1-4** may originate from the σ(Ru-O)π*(R-bpy) transition. With the increase of the electron-withdrawing ability of the R group, π*(R-bpy) orbital is stabilized more efficiently and thus σ(Ru-O)π*(R-bpy) state will be accessed more easily from the MLCT states.

It is worth noting that we observed remarkable wavelength dependence of the Ru-O homolysis. When **4** was irradiated with 532 nm laser, no seven-line EPR signal was observed except for a weak background signal, though the laser intensity at 532 nm was tuned to the same as or even stronger than that at 355 nm and the OD values of the samples were kept constant at 355 and 532 nm (Figure S9). The phenomena hint at that the σ(Ru-O)π*(R-bpy) state may be reached through the high-lying ^{1}MLCT or ^{3}MLCT states rather than the lowest-lying ^{1}MLCT or ^{3}MLCT states.[18]

Theoretical calculations

Computational studies were undertaken to gain further understanding of the substituent effects observed in ligand exchange and radical generation. All calculations were performed with the Gaussian 09[19] (G09) program package employing the density functional theory (DFT) method with Becke's three-parameter hybrid functional and LeeYang-Parr's gradient corrected correlation functional (B3LYP).[20] The SDD basis set[21] and effective core potential were used for the Ru atom, and the 6-31 G* basis set was applied for H, C, N, O and S.[22] The calculated molecular orbital diagrams of **1-4** are shown in Figure 4. The lowest unoccupied molecular orbital (LUMO) and LUMO+1 of each complex are R-bpy based π* in character, while the highest occupied molecular orbital (HOMO), HOMO-

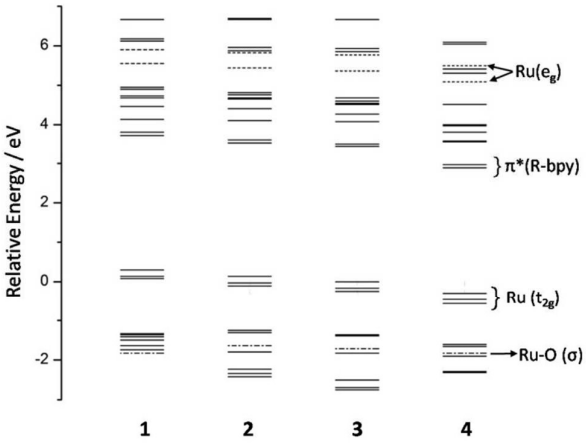

Figure 4. Molecular orbital diagrams of **1-4**, where dashed lines represent Ru(e_g) and Ru-O (σ) orbitals, respectively. The HOMO of **3** is set at 0.0 eV as an arbitrary reference.

1 and HOMO-2 of each complex are mainly centered on the metal and assignable to the Ru(t_{2g}) orbitals (Figure 4 and Figure S10). The energy levels of both HOMO and LUMO show a decreased tendency from **1** to **4**, which agrees very well with the anodic shift of the Ru-based oxidation potentials and R-bpy-based reduction potentials from **1-4** (Table 1). The two e_g-type orbitals (^{3}LF states) with Ru-L(σ*) character, which are generally believed to account for ligand dissociation,[23] are calculated as LUMO+8 and LUMO+9 in **1-3**, and LUMO+8 and LUMO+11 in **4**.

It is widely accepted that the photoinduced ligand dissociation of the Ru complexes occurs from the ^{3}LF states via thermal population from the lowest-lying ^{3}MLCT states.[23] Recently, ^{3}LF state population directly through ^{1}MLCT states was also proposed to be possible.[8a,18] TD-DFT calculations (based on the optimized ground state geometry, Table S1-S4) reveal that the lowest triplet states of **1-4** are ^{3}MLCT states, with transition maxima at 529 nm (2.34 eV) for **1**, 545 nm (2.27 eV) for **2**, 543 nm (2.28 eV) for **3** and 602 nm (2.06 eV) for **4**, respectively. The calculated first and second ^{3}LF states locate at 2.51 and 2.92 eV for **1**, 2.56 and 3.03 eV for **2**, 2.59 and 3.05 eV for **3**, and 2.63 and 2.87 eV for **4**. To lose py-SO_3 bidentate ligand, both ^{3}LF state should be accessed simultaneously.[24] If ^{3}LF states are populated via the lowest-lying ^{3}MLCT, **1** should undergo ligand dissociation most efficiently because it has the smallest energy gap between the second ^{3}LF and the lowest-lying ^{3}MLCT (0.58, 0.76, 0.77 and 0.81 eV for **1-4**). In fact, the ligand dissociation quantum yield of **1** is the smallest one, implying ^{3}LF states may be partially accessed from the high-lying ^{1,3}MLCT or vibrationally excited lowest-lying ^{3}MLCT. Thus, the energy gap and orbital overlap of the ^{3}LF states with these states may determine their population efficiencies, which, in combination with the solvent-cage effect, finally lead to the observed ligand dissociation order of **1** < **2** < **3** > **4** (Table 1).

To understand the py-SO_3· radical generation abilities of **1-4** upon 355 nm irradiation, we then put our attention on the excited states with the σ(Ru-O) to π*(R-bpy) transition character. The calculations reveal that the σ(Ru-O) orbitals lie below the metal-based t_{2g} orbitals, assigned to HOMO-9 for **1** and HOMO-5 for **2**, **3**, and **4**, respectively. This attribution is supported by the fact that the oxygen atom that coordinates to the Ru center gives the greatest contribution in these orbitals (Table S5). Meanwhile, these orbitals have significant Ru-O covalent bonding character (Figure S11).[25] For **1**, though HOMO-5 shows a high contribution from bonded O atom, no obvious Ru-O covalent bonding character is observed (Figure S12). The σ(Ru-O) orbitals of **1-4** lie at -1.82, -1.63, -1.71 and -1.82 eV with respect to the HOMO of **3**, which was set at 0.0 eV as an arbitrary reference (Figure 4). The calculations suggest that the substituents on bpy ligands have less effects on σ(Ru-O) orbitals than on π*(R-bpy) orbitals (Figure 4), in line with the common knowledge.

With the assignment of σ(Ru-O) orbitals in hand, the energy levels of σ(Ru-O)π*(R-bpy) states may be figured out, as shown in Table S1-S4. The calculated triplet excited states with significant contribution from σ(Ru-O)π*(R-bpy) occur at 286, 286, 279 and 307 nm for **1-4**, respectively. Clearly, the electron-withdrawing substituent in **4** brings the σ(Ru-O)π*(R-bpy) state to a much lower energy region, favoring its population from the high-lying MLCT states. Additionally, the contributions of σ(Ru-O)π*(R-bpy) transition in these triplet excited states are, respectively, 3% for **1**, 9% for **2**, 27% for **3**, and 20% for **4** (Table S1-S4). These factors may provide a reasonable explanation for the radical generation abilities of **4** > **3** > **2** > **1** observed in EPR experiments. Due to the lowest σ(Ru-O)π*(R-bpy) transition energy and moderate transition contribution, **4** becomes the most effective one in py-SO_3· generation.

What worthy of noting is that the calculated triplet energy levels of σ(Ru-O)π*(R-bpy) transitions may be overestimated, which can be deduced from the comparison of the calculated ^{3}MLCT to the measured one. The lowest ^{3}MLCT states estimated from the emission spectra at 77 K localize at 640 nm for **1**, 630 nm for **2**, 620 nm for **3,** and 660 nm for **4**, which are

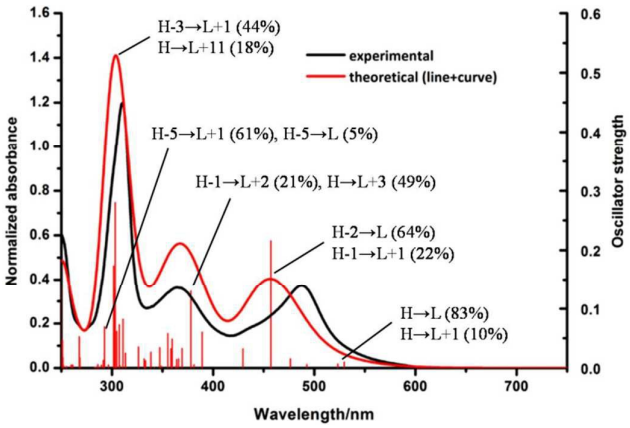

Figure 5. Normalized experimental and theoretical absorption spectra of **4** in H_2O. MO contributions and transition energies were calculated using TD-DFT and only select contributions greater than 5% are assigned (H = HOMO, L = LUMO).

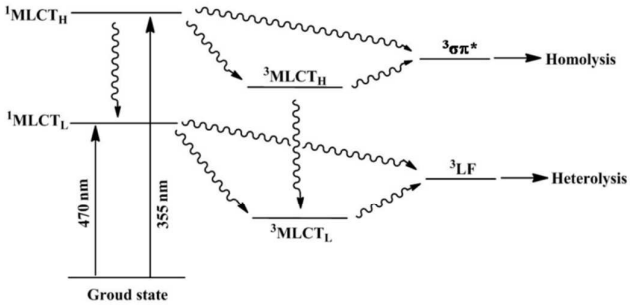

Figure 6. Simplified Jablonski diagram for **4**. $MLCT_L$ and $MLCT_H$ denote the MLCT state in low and high energy level, respectively.

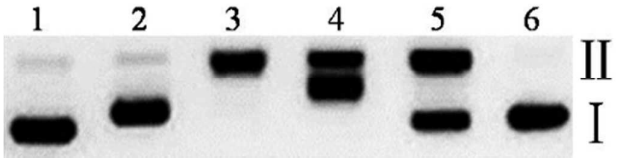

Figure 7. Agarose gel electrophoresis pattern of pBR322 DNA (100 mM in base pairs) in Ar-saturated Tris-EDTA (5 mM, pH = 7.5) upon irradiation (355 nm laser, 90 mW) for 8 min in the presence of varied concentrations of **4**. Lane 1, DNA alone; lane 2, 5 μM; lane 3, 10 μM; lane 4, 20 μM; lane 5, $[Ru(bpy)_3]^{2+}$ (100 μM), air-saturated, 470 nm LED, 15 W, 15 min); lane 6, 50 μM (dark). I and II denote supercoiled circular and nicked circular plasmid DNA, respectively.

red shifted by 60~110 nm than the calculated results. Taking this in mind, the population of $^3\sigma$(Ru-O)π^*(R-bpy) states by way of high-lying ^{1}MLCT or ^{3}MLCT should be thermodynamically allowed upon excitation at 355 nm, but might not at 532 nm, which can populate the lowest-lying ^{1}MLCT and ^{3}MLCT states only.

We then theoretically examined the possibility of direct excitation of the $^1\sigma$(Ru-O)π^*(R-bpy) state. Thus, the singlet excited state properties of **1-4** were calculated using TD-DFT. As shown in Figure 5 and Figure S13-15, the lowest vertical singlet excited states of **1-4** mainly belong to HOMO→LUMO transitions, with oscillator strengths (*f*) smaller than 0.01 (Table S6-S9). More intense absorption bands with (f > 0.1) occur at 428 nm (f = 0.1105) for **1**, 430 nm (f = 0.1528) for **2**, 425 nm (f = 0.1285) for **3**, and 457 nm (f = 0.2160) for **4**, with main contributions from HOMO-2→LUMO and HOMO-1→LUMO+1 transitions. These calculated ^{1}MLCT maxima are in good agreement with the experimental values, 467 nm for **1**, 458 nm for **2**, 452 nm for **3**, and 488 nm for **4** (Figure 1, Table1). The $^1\sigma$(Ru-O)π^*(R-bpy) transitions are predicted at 248 nm (f = 0.0381) for **1**, 264 nm (f = 0.0222) for **2**, 269 nm (f = 0.0513) for **3**, and 293 nm (f = 0.0695) for **4**, respectively, indicating that the direct excitation population of the $^1\sigma$(Ru-O)π^*(R-bpy) states is only possible under irradiation with λ < 300 nm. As a result, the $^3\sigma$(Ru-O)π^*(R-bpy) state in our experiments should either come from a high-lying ^{1}MLCT state via intersystem crossing (isc) or from a high-lying ^{3}MLCT state via internal conversion (ic) or both processes.

Combining the experimental and theoretical results, a simplified Jablonski diagram for complex **4** is put forward as shown in Figure 6. Excitation with visible light of 470 nm populates the low-lying ^{1}MLCT (^{1}MLCT$_L$), and then low-lying ^{3}MLCT (^{3}MLCT$_L$) via isc. The ^{3}LF may be populated either from ^{3}MLCT$_L$ by thermal activation or from ^{1}MLCT$_L$ directly,[8a] resulting in the bidentate ligand dissociation. When excited at 355 nm, high-lying ^{1}MLCT (^{1}MLCT$_H$) and ^{3}MLCT (^{3}MLCT$_H$) may be populated, by which the $^3\sigma$(Ru-O)π^*(R-bpy) state is accessed to result in the Ru-O homolysis and the formation of py-SO_3· radicals.

Photoinduced DNA binding and cleavage

Gel electrophoresis assays were carried out to validate the EPR and calculation results. It is anticipated that **1-4** can covalently bind DNA and cleave DNA simultaneously upon 355 nm irradiation, as the result of both ligand dissociation and ROS generation (including py-SO_3· and ·OH, both can be generated in hypoxic conditions[10]). In contrast, 470 nm irradiation will mainly give rise to the covalent binding of DNA due to the decline or loss of the ROS generation ability. As shown in Figure 7, **4** covalently bond DNA at low concentration upon 355 nm laser excitation as evidenced by DNA mobility retardation (lane 2), and cleaved DNA at higher concentrations as evidenced by the appearance of the nicked circular (lane 3) and even linear DNA (lane 4). Whereas, only decreased DNA migration was observed when taking a 470 nm LED in place of the 355 nm laser (Figure S16). Similar experiments were also carried out in the cases of **1-3** (Figure S17-S22). **3** behaved very similarly to **4** (Figure S17-S18). In contrast, **1** and **2** can only covalently bind DNA even upon 355 nm irradiation (Figure S19-S22), probably due to their poor ROS generation abilities, in accord with the EPR and calculation results.

Conclusions

The photoinduced radical generation via the Ru-O homolysis in **1-4** was investigated experimentally and theoretically**.** All of the complexes underwent rapid py-SO_3 dissociation upon visible light irradiation (470 nm). EPR experiments demonstrate that 355 nm irradiation may lead to Ru-O homolysis and py-SO_3· radical generation in Ar-saturated CH_3CN, but 532 nm irradiation cannot. The Ru-O homolysis followed the order of **4** > **3** > **2** > **1**. DNA electrophoresis assays reveal that **3** and **4** may give rise to both DNA covalent binding and cleavage upon 355 nm irradiation under hypoxic conditions, but only DNA covalent binding upon 470 nm irradiation. In contrast, **1** and **2** can only covalently bind DNA irrespective of 355 or 470 nm irradiation. The high Ru-O homolysis efficiency of **4** and its wavelength dependence may be rationalized by regarding the $^3\sigma$(Ru-O)π^*(R-bpy) state as the origin of the Ru-O homolysis, which is supported by TD-DFT calculations. Inspired by this work, bpy modification with stronger electron-withdrawing group and py-SO_3 modification

by electron-donating group are underway, both strategies may stabilize the $^3\sigma$(Ru-O)π^*(R-bpy) state and enhance the Ru-O homolysis efficiency further.

Experimental section

Materials. $RuCl_3.3H_2O$, 4,4'-dimethoxy-2,2'-bipyridine (L_1), 4,4'-dimethyl-2,2'-bipyridine (L_2), 2,2'-bipyridine (L_3), dimethyl [2,2'-bipyridine]-4,4'-dicarboxylate (L_4), 2-pyridinesulfonic acid, DMPO (5,5-dimethyl-1-pyrroline-*N*-oxide), gel loading buffer and trishydroxymethyl- aminomethane (Tris base) were purchased from Sigma Aldrich. The supercoiled pBR322 plasmid DNA was obtained from TaKaRa Biotechology Company. *Cis*-Ru(4,4'-$(R)_2$-2,2'-bipyridine)Cl_2 (R = OCH_3, CH_3, H, $COOCH_3$) were synthesized following the reported methods[26] and *Cis*-[Ru(4,4'-$(R)_2$-2,2'-bipyridine)(py-SO_3)](PF_6) were prepared by our reported procedures.[10]

[$Ru(L_1)_2$(py-SO_3)](PF_6) (**1**). ^{1}H NMR (400 MHz, d_6-acetone) δ 9.02 (d, *J* = 6.5 Hz, 1H), 8.30 (m, 4H), 8.17 (d, *J* = 6.5 Hz, 1H), 8.06 (t, *J* = 7.7 Hz, 1H), 7.87 (d, *J* = 7.8 Hz, 1H), 7.75 (d, *J* = 6.6 Hz, 1H), 7.63 (m, 2H), 7.49 – 7.38 (m, 2H), 7.24 (m, 1H), 7.01 (m, 2H), 4.12 (s, 6H), 4.02 (d, *J* = 3.4 Hz, 6H) (Figure S23).HR ESI-MS: m/z = 692.0727 for $(M\text{-}PF_6)^+$ (Figure S24)**.** Anal. Calcd for $C_{29}H_{28}F_6N_5O_7PRuS{\cdot}2H_2O$: C, 39.91; H, 3.70; N, 8.02. Found: C, 39.85; H, 3.73; N, 7.96.

[$Ru(L_2)_2$(py-SO_3)](PF_6) (**2**).^{1}H NMR (400 MHz, d_6-acetone) δ (ppm) 9.09 (d, *J* = 5.8 Hz, 1H), 8.64 (s, 1H), 8.57 (s, 2H), 8.52 (s, 1H), 8.24 (d, *J* = 5.8 Hz, 1H), 8.09 (t, *J* = 7.7 Hz, 1H), 7.90 (d, *J* = 7.8 Hz, 1H), 7.79 (d, *J* = 5.9 Hz, 1H), 7.68 (d, *J* = 5.6 Hz, 1H), 7.62 (d, *J* = 5.8 Hz, 1H), 7.55 (d, *J* = 5.4 Hz, 1H), 7.48 (d, *J* = 5.6 Hz, 1H), 7.42 (t, *J* = 6.6 Hz, 1H), 7.23 (d, *J* = 2.8 Hz, 2H), 2.65 (d, *J* = 4.9 Hz, 6H), 2.51 (d, *J* = 8.3 Hz, 6H) (Figure S23).HR ESI-MS: m/z = 628.0944 for $(M\text{-}PF_6)^+$ (Figure S24)**.** Anal. Calcd for $C_{29}H_{28}F_6N_5O_3PRuS{\cdot}2H_2O$: C, 43.07; H, 3.99; N, 8.66. Found: C, 43.01; H, 4.05; N, 8.61.

[$Ru(L_4)_2$(py-SO_3)](PF_6) (**4**).^{1}H NMR (400 MHz, d_6-acetone) δ (ppm) 9.42 (d, *J* = 5.8 Hz, 1H), 9.36 (s, 1H), 9.31 (s, 1H), 9.26 (d, *J* = 1.6 Hz, 1H), 9.24 (d, *J* = 1.4 Hz, 1H), 8.71 (d, *J* = 5.8 Hz, 1H), 8.41 – 8.35 (m, 2H), 8.21 – 8.09 (m, 3H), 7.98 (d, *J* = 7.8 Hz, 1H), 7.79 (m, 2H), 7.63 (d, *J* = 5.5 Hz, 1H), 7.50 – 7.44 (m, 1H), 4.07 (d, *J* = 3.9 Hz, 6H), 3.97 (s, 6H) (Figure S23).HR ESI-MS: m/z = 804.0631 for $(M\text{-}PF_6)^+$ (Figure S24)**.** Anal. Calcd for $C_{33}H_{28}F_6N_5O_{11}PRuS{\cdot}2H_2O$: C, 40.25; H, 3.28; N, 7.11. Found: C, 40.22; H, 3.25; N, 7.12.

Acknowledgements

This work was financially supported by the Ministry of Science and Technology (2013CB933801) and NSFC (21390400, 21172228, 21273259, 21571181, 21301182). We also appreciated the funding and technical support from Shanghai Supercomputer Center in DFT calculations.

Notes and references

1 (a) G. Sava, A. Bergamo and P. J. Dyson, *Dalton Trans.*, 2011, 40, 9069-9075; (b) N. J. Wheate, S. Walker, G. E. Craig and R. Oun, *Dalton Trans*., 2010, 39, 8113-8127; (c) C. G. Hartinger and P. J. Dyson, *Chem. Soc. Rev*., 2009, 38, 391-401; (d) E. R. Jamieson and S. J. Lippard, *Chem. Rev*., 1999, 99, 2467-2498.

2 (a) E. Gabano, M. Ravera and D. Osella, *Dalton Trans.*, 2014, **43**, 9813-9820; (b) R. K. Pathak, S. Marrache, J. H. Choi, T. B. Berding and S. Dhar, *Angew. Chem. Int. Ed.*, 2014, **53,** 1963-1967; (c) Y.-R. Zheng, K. Suntharalingam, T. C. Johnstone, H. Yoo, W. Lin, J. G. Brooks and S. J. Lippard, *J. Am. Chem. Soc.*, 2014, **136**, 8790-8798; (d) E. Wexselblatt and D. Gibson, *J. Inorg. Biochem.*, 2012, **117**, 220-229.

3 (a) A. Gandioso, E. Shaili, A. Massaguer, G. Artigas, A. González-Cantó, J. A. Woods, P. J. Sadler and V. Marchán, *Chem. Commun*., 2015, **51**, 9169-9172; (b) G. Thiabaud, J. F. Arambula, Z. H. Siddik and J. L. Sessler, *Chem. Eur. J*., 2014, **20**, 8942-8947; (c) N. J. Farrer, J. A. Woods, L. Salassa, Y. Zhao, K. S. Robinson, G. Clarkson, F. S. Mackay and P. J. Sadler, *Angew. Chem. Int. Ed*., 2010, **49**, 8905-8908; (d) F. S. Mackay, J. A. Woods, P. Heringova, J. Kašpárková, A. M. Pizarro, S. A. Moggach, S. Parsons, V. Brabec and P. J. Sadler, *PNAS*, 2007, **104**, 20743-20748; (e) F. S. Mackay, J. A. Woods, H.Moseley, J. Ferguson, A. Dawson, S. Parsons and P. J. Sadler, *Chem. Eur. J.*, 2006, **12**, 3155-3161.

4 (a) K. D. Mjos and C. Orvig, *Chem. Rev*., 2014, **114**, 4540-4563; (b) N. P. E. Barry and P. J. Sadler, *Chem. Commun*., 2013, **49**, 5106-5131; (c) D. Gaynor and D. M. Griffith, *Dalton Trans*., 2012, **41**, 13239-13257; (d) C. G. Hartinger and P. J. Dyson, *Chem. Soc. Rev*., 2009, **38**, 391-401; (e) T. Gianferrara, I. Bratsos and E. Alessio, *Dalton Trans*., 2009, 7588-7598.

5 (a) M. Alagesan, P. Sathyadevi, P. Krishnamoorthy, N. S. P. Bhuvaneshb and N. Dharmaraj, *Dalton Trans*., 2014, **43**, 15829-15840; (b) F. Caruso, M. Rossi, A. Benson, C. Opazo, D. Freedman, E. Monti, M. B. Gariboldi, J. Shaulky, F. Marchetti, R. Pettinari, C. Pettinari, *J. Med. Chem.,* 2012, **55**, 1072-1081; (c) P. J. Dyson and G. Sava, *J. Chem. Soc.*, *Dalton Trans*., 2006, 1929-1933.

6 (a) Q. Zhou, Y. Zheng, T. Wang, Y. Chen, K. Li, Y. Zhang, C. Li, Y. Houa and X. Wang, *Chem. Commun*., 2015, **51**, 10684-10686; (b) M. A. Sgambellone, A. David, R. N. Garner, K. R. Dunbar and C. Turro, *J. Am. Chem. Soc*., 2013, **135**, 11274-11282; (c) S. Betanzos-Lara, L. Salassa, A. Habtemariam, O. Novakova, A. M. Pizarro, G. J. Clarkson, B. Liskova, V. Brabec and P. J. Sadler, *Organometallics*, 2012, **31**, 3466-3479; (d) B. S. Howerton, D. K. Heidary and E. C. Glazer, *J. Am. Chem. Soc.*, 2012, **134**, 8324-8327; (e) E. Wachter, D. K. Heidary, B. S. Howerton, S. Parkin and E. C. Glazer, *Chem. Commun*., 2012, **48**, 9649-9651; (f) R. N. Garner, J. C. Gallucci, K. R. Dunbar and C. Turro, *Inorg. Chem*., 2011, **50**, 9213-9215; (g) F. Barragán, P. López-Senín, L. Salassa, S. Betanzos-Lara, A. Habtermariam, V. Moreno, P. J. Sadler and V. Marchán, *J. Am. Chem. Soc*., 2011, **133**, 14098-14108; (h) R. E. Goldbach, I. Rodriguez-Garcia, J. H. van Lenthe, M. A. Siegler and S. Bonnet, *Chem. Eur. J.*, 2011, **17**, 9924-9929; (i) S. J. Berners-Price, *Angew. Chem., Int. Ed*., 2011, **50**, 804–805; (j) S. Betanzos-Lara, L. Salassa,A. Habtemariam and P. J. Sadler, *Chem. Commun*., 2009, 6622-6624.

7 (a) W.-Q. Cao, W.-J. Zheng and T.-F. Chen, *Sci. Rep*., 2015, **5**, 9157; (b) B. A. Albani, B. Peña, N. A. Leed, N. A. B. G. de Paula, C. Pavani, M. S. Baptista, K. R. Dunbar and C. Turro, *J. Am. Chem. Soc.*, 2014, **136**, 17095-17101.

8 (a) J. D. Knoll, B. A. Albani and C. Turro, *Acc. Chem. Res.,* 2015, **48**, 2280-2287; (b) J. D. Knoll, B. A. Albani and C. Turro, *Chem. Commun*., 2015, **51**, 8777-8780; (c) Y. Chen, W. Lei, Y. Hou, C. Li, G. Jiang, B. Zhang, Q. Zhou and X. Wang, *Dalton Trans.*, **2015**, *44*, 7347-7354; (d) Y. Chen, W. Lei, G. Jiang, Y. Hou, C. Li, B. Zhang, Q. Zhou and X. Wang, *Dalton Trans.*, **2014**, *43*, 15375-15384; (e) B. A. Albani, B. Peña, N. A. Leed,

N. A. B. G. de Paula, C. Pavani, M. S. Baptista, K. R. Dunbar and C. Turro, *J. Am. Chem. Soc*., 2014, **136**, 17095-17101.
9 (a) M. R. Detty, S. L. Gibson and S. J. Wagner, *J. Med. Chem.*, 2004, **47**, 3897-3915; (b) D. E. J. G. J. Dolmans, D. Fukumura and P. K. Jain, *Nat. Rev. Cancer,* 2003, **3**, 380-387.
10 Y. Zheng, Q. Zhou, W. Lei, Y. Hou, K. Li, Y. Chen, B. Zhang and X. Wang, *Chem. Commun*., 2015, **51**, 428-430.
11 T. K. Janaratne, A. Yadav, F. Ongeri and F. M. MacDonnell, *Inorg. Chem*., 2007, **46**, 3420-3422.
12 (a) K. Cory MacLeod, J. L. Conway, B. O. Patrick and K. M. Smith, *J. Am. Chem. Soc.*, 2010, **132**, 17325-17334; (b) A. J. Brooks, M. Vlasie, R. Banerjee and T. C. Brunold, *J. Am. Chem.*
Soc., 2005, **127**, 16522-16528; (c) M. D. Vlasie and R. Banerjee, *J. Am. Chem. Soc*., 2003, **125**, 5431-5435; (d) D. C. Woska, Z. D. Xie, A. A. Gridnev,S. D. Ittel, M. Fryd and B. B. Wayland, *J. Am. Chem. Soc*., 1996, **118**, 9102-9109.
13 (a) B. D. Rossenaar, C. J. Kleverlaan, M. C. E. van de Ven, D. J. Stufkens, A. Vlček, Jr. *Chem. Eur. J.,* 1996, **2**, 228-237; (b) C. J. Kleverlaan, D. M. Martino, H. Willigen., D. J. Stufkens, A. Oskam. *J. Phys. Chem*., 1996, **100**, 18607-18611; (c) B. D. Rossenaar, M. W. George, Frank P. A. Johnson, Derk J. Stufkens, James J. Turner, Antonin Vlček, Jr. *J. Am. Chem. Soc.*, 1995, **117**, 11582-11583; (d) H. A. Nieuwenhuis, M. C. E. van de Ven, D. J. Stufkens, A. Oskam, K. Goubitz, *Organometallics*, 1995, **14**, 780-788.
14 M. Maestri, N. Armaroli, V. Balzani, E. C. Constable, and A. M. W. C. Thompson. *Inorg. Chem*., 1995, **34**, 2159-2161.
15 (a) M. J. Root, B. P. Sullivan, T. J. Meyer, E. Deutsch. *Inorg. Chem.*, 1985, **24**, 2731-2739; (b) N. Aydin; C.W.Schlaepfer. *Polyhedron*, 2001, **20**, 37-45.
16 (a) R. N. Garner, L. E. Joyce and C. Turro, *Inorg. Chem.*, 2011, **50**, 4384-4391. (b) B. Durham, S. R. Wilson, D. J. Hodgson and T. J. Meyer, *J. Am. Chem. Soc.*, 1980, **102**, 600-607.
17 G. M. Rosen and E. J. Rauckman, *Mol. Pharmacol.*, 1979, **17**, 233-238.
18 (a) Y. Liu, D. B. Turner, T. N. Singh, A. M. Angeles-Boza, A. Chouai, K. R. Dunbar and C. Turro, *J. Am. Chem. Soc.,* 2009, **131**, 26-27; (b) W. M. Wacholtz, R. A. Auerbach, R. H. Schmehl, M. Ollino and W. R. Cherry, *Inorg. Chem*., 1985, **24**, 1758-1760.
19 M. J. Frisch, G. W. Trucks, H. B. Schlegel, G. E. Scuseria, M. A. Robb, J. R. Cheeseman, G. Scalmani, V. Barone, B. Mennucci, G. A. Petersson, H. Nakatsuji, M. Caricato, X. Li, H. P. Hratchian, A. F. Izmaylov, J. Bloino, G. Zheng, J. L. Sonnenberg, M. Hada, M. Ehara, K. Toyota, R. Fukuda, J. Hasegawa, M. Ishida, T. Nakajima, Y. Honda, O. Kitao, H. Nakai, T. Vreven, J. A. Montgomery Jr., J. E. Peralta, F. Ogliaro, M. Bearpark, J. J. Heyd, E. Brothers, K. N. Kudin, V. N. Staroverov, R. Kobayashi, J. Normand, K. Raghavachari, A. Rendell, J. C. Burant, S. S. Iyengar, J. Tomasi, M. Cossi, N. Rega, J. M. Millam, M. Klene, J. E. Knox, J. B. Cross, V. Bakken, C. Adamo, J. Jaramillo, R. Gomperts, R. E. Stratmann, O. Yazyev, A. J. Austin, R. Cammi, C. Pomelli, J. W. Ochterski, R. L. Martin, K. Morokuma, V. G. Zakrzewski, G. A. Voth, P. Salvador, J. J. Dannenberg, S. Dapprich, A. D. Daniels, Ö. Farkas, J. B. Foresman, J. V. Ortiz, J. Cioslowski, D. J. Fox, *Gaussian 09*, revision A.1, Gaussian, Inc., Wallingford, CT, **2009**.
20 (a) A. D. Becke, *J. Chem. Phys.* 1993, **98**, 5648-5652. (b) C. Lee, W. Yang and R. G. Parr, *Phys. Rev. B: Condens. Matter*. 1988, **37**, 785-789.
21 L. E. Roy, P. J. Hay and R. L. Martin. *J. Chem. Theory Comput.* 2008**, 4**, 1029-1031.
22 (a) P. C. Harihara and J. A. Pople, *Theor. Chim. Acta*, 1973, **28**, 213-222; (b) M. M. Francl, W. J. Pietro, W. J. Hehre, J. S. Binkley, M. S. Gordon, D. J. Defrees and J. A. Pople, *J. Chem. Phys.* 1982, **77**, 3654-3665.
23 (a) P. C. Ford , Coord. *Chem. Rev.*, 1982, **44**, 61–82. (b) P. C. Ford, D. Wink, J. Dibenedetto, *Prog. Inorg. Chem.,* 1983, **30**, 213–271. (c) E. Tfouni, *Coord. Chem. Rev.*, 2000, **196**, 281–305.
24 B. A. Albani, B. Peña, K. R. Dunbar., C. Turro. *Photochem. Photobiol. Sci.*, 2014, **13**, 272.
25 (a) S. Bellinger-Buckley, T.C. Chang, S. Bag, D. Schweinfurth, W. H. Zhou, B. Torok, B. Sarkar, M.K. Tsai and J. Rochford, *Inorg. Chem.*, 2014, **53**, 5556-5567; (b) H. C. Zhao, B. L. Fu, D. Schweinfurth, J. P. Harney, B. Sarkar, M.K. Tsai and J. Rochford, *Eur. J. Inorg. Chem.,* **2013**, 4410-4420.
26 B. P. Sullivan, D. J. Salmon, T. J. Meyer, *Inorg. Chem*., 1978, **17**, 3334-3341.

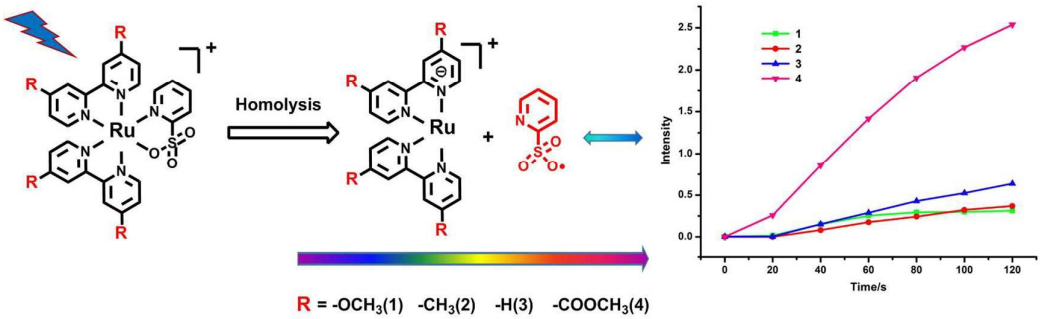

Electron-withdrawing substituents on the bpy ligands improve the photoinduced Ru-O homolysis in the $[Ru(bpy)_2(py\text{-}SO_3)]^+$–type complexes.